Korean J. Chem. Eng., 33(12), 3541-3549 (2016)
DOI: 10.1007/s11814-016-0219-y

pISSN: 0256-1115
eISSN: 1975-7220

Rapid and effective removal of sodium lignosulfonate from aqueous solutions by in-situ formed magnesium hydroxide

Lanlan Ye*, Feng Li*, Tao Wu,†, and Yujiang Li*,†**

*Shandong Provincial Key Laboratory of Water Pollution Control and Resource Reuse, School of Environmental Science & Engineering, Shandong University, Jinan 250100, P. R. China
**Key Laboratory of Colloid & Interface Science of Education Ministry, Shandong University, Jinan 250100, P. R. China
(*Received 18 April 2016 • accepted 30 July 2016*)

Abstract−We investigated the efficiency of in-situ formed magnesium hydroxide ($Mg(OH)_2$) for the removal of sodium lignosulfonate (SLSN) from aqueous solution. Adsorption experiments considered the effects of various conditions such as pH, $MgCl_2$ concentration, contact time, and temperature on SLSN removal efficiency. It was found that approximately 93%-99% SLSN was removed by in-situ formed $Mg(OH)_2$. The adsorption was rapid, and the contact time required to reach complete adsorption equilibrium was less than 2 min. Moreover, that the $Mg(OH)_2$ lost about 0.5-3.0% adsorption capacity for SLSN when NO_3^-, HCO_3^-, $H_2PO_4^-$ and SO_4^{2-} anions were simultaneously present with SLSN. The experimental data suggested that there was little competitive adsorption of SLSN with other coexisting anions on $Mg(OH)_2$. The co-precipitation/adsorption process was exothermic and physical, involving weak interactions such as electrostatic attraction, hydrogen bonding, adhesive forces, and van der Waals forces between SLSN molecules and the binding sites on $Mg(OH)_2$.

Keywords: In-situ, Adsorption, Surfactant, Particles

INTRODUCTION

Surfactants are surface/interface active substances designed for lowering the surface/interface tension [1,2]. They commonly contain oxygen, sulfur, and nitrogen atoms in their headgroups and thus headgroups are well solvated in water, while non-polar hydrocarbon tails of surfactants are not easily dissolved in water [2]. In this case, surfactant molecules are amphipathic. Surfactants are mainly divided into four groups: anionic, non-ionic, zwitterionic, and cationic surfactants [1-4]. Among these, anionic surfactants are one of the most extensively applied surfactants [1-4]. Surfactants are widely used in households and industries including oil recovery, mining, pesticide formulations, dye printing, paints, detergents, personal care products, and pulp and paper industries [1-4]. With the increasing demand for energy around the world and diminishing amount of conventional oil, it is very important to explore new techniques for enhanced oil recovery (EOR) [2]. With the development of tertiary oil recovery, more and more EOR processes have been carried out to increase oil recovery and stabilize oil production. In EOR processes, higher oil recovery is achieved by using chemicals such as alkalis, surfactants, and polymers. Alkalis are intended to in-situ generate surfactants by reacting with acidic components in the crude oil and reduce interfacial tension (IFT) between oil and aqueous phases [5]. Surfactants are designed for lowering the IFT, changing the wettability, and promoting residual oil mobility to overcome the capillary forces [5-8]. Therefore, surfactants play an important role in EOR processes. Anionic surfactants such as petroleum sulfonate and lignosulphonate have been widely employed for common surfactant flooding or alkali/surfactant/polymer (ASP) flooding due to their low-cost, availability, and solubility in water [9]. During crude oil and natural gas production processes, large quantities of liquid waste are being generated by the surfactant flooding or ASP flooding. Such liquid waste is called produced water. Even though most of the floating pollutants are separated from produced water, residual anionic surfactants and their degradation products cannot be removed effectively by oil-water separation techniques and remain in the produced water due to their high solubility in water, leading to the formation of stable oil-in-water (O/W) emulsions, which is a challenge for the petroleum industry [10]. Because surfactant molecules have surface/interface activity, they can rapidly adsorb at the oil-water interface or the surface of oil droplets and form elastic interface film, which protects the oil droplets against coalescence [11]. In this case, the produced water becomes very stable. In particular, the separation of residual oil from produced water is more difficult. Therefore, rapid and effective removal of anionic surfactants from aqueous solution becomes a necessity for the successful application of surfactant flooding or ASP flooding techniques.

Sodium lignosulfonate (SLSN) is an important anionic surfactant and dispersant with extensive sources and lower cost that has been widely used in EOR processes, pulp and paper industries. To our knowledge, SLSN as a class of anionic surfactant, has not been extensively studies [4,12-16]. A few studies have focused on the adsorption of SLSN on the oppositely charged solid particles. A full understanding of the adsorption behavior of the surfactant molecules at the solid-liquid interface can help to remove SLSN

†To whom correspondence should be addressed.
E-mail: yujiang@sdu.edu.cn, wutao@sdu.edu.cn

from aqueous solution.

$Mg(OH)_2$ has attracted increasing attention due to its wide applications, including antacids, adsorbents [17], fertilizer additives [17], filler materials [18], precursors for magnesium oxide [19], flame retardants [20], and smoke suppressants [21]. $Mg(OH)_2$ has a layered crystal structure; such layered metal hydroxides have attractive features, for example, a larger specific surface area and a higher positive charge density of the layers, which contributes to a higher reactivity [22]. Several methods have been used to prepare $Mg(OH)_2$ with controlled shape and size [19,23-25]. Some studies have reported the synthesis of nano-sized $Mg(OH)_2$ by hydrothermal [26], sol-gel [27], and solvothermal [28]. However, these methods require complicated operating conditions or longer synthesis time, which makes them not practical for industrial production [29].

We used the in-situ wet precipitation method to prepare $Mg(OH)_2$ particles because it is simple, low cost and suitable for industrial processing. $MgCl_2$ and SLSN solutions were initially present in the reactor at a controlled temperature, and the $Mg(OH)_2$ particles were obtained by the addition of alkali into the reactor. The in-situ formed $Mg(OH)_2$ particles were used as effective adsorbents to remove SLSN from aqueous solution. We used SLSN as model anionic surfactant to investigate the interactions between SLSN molecules and oppositely charged $Mg(OH)_2$ particles. The effects of adsorption parameters such as solution pH, $MgCl_2$ concentration, contact time, and temperature on the adsorption efficiency were investigated. The related reaction mechanism was also discussed.

MATERIALS AND METHODS

1. Materials

Analytical reagent (AR) grade magnesium chloride hexahydrate ($MgCl_2 \cdot 6H_2O$) and sodium hydroxide (NaOH) were purchased from Sinopharm Chemical Reagent Co., Ltd. (Shanghai, China). Sodium lignosulfonate (SLSN, >98%) was purchased from TCL Development Co., Ltd. (Shanghai, China) and used without further purification. All other reagents were of analytical grade.

2. Preparation of $Mg(OH)_2$ Particles

$Mg(OH)_2$ particles were synthesized with the following procedures: 20 mL of 2.0 g/L NaOH solution was dropped into 20 mL of 2.0 g/L $MgCl_2$ solution. Temperature (25 °C) and pH (10.5±0.1) were kept constant with stirring during the addition of NaOH solution to the mixed aqueous solution.

3. Characterization

The morphology and structure of the in-situ formed $Mg(OH)_2$ with and without SLSN were characterized by an AIS-2100 scanning electron microscope (SEM, MIRERO-SERON, Republic of Korea) and a JEM-2100 high-resolution transmission electron microscope (HRTEM, JEOL Ltd., Japan). The crystal structure of samples was characterized by a D/Max-rB power diffraction (XRD, Rigaku, Japan) using Cu-Kα radiation source in the 2θ range of 2°-70° with a scanning rate of 2°/min. The chemical bonds and surface functional groups of the samples were recorded on a Perkin-Elmer Fourier transform infrared spectrometer (FT-IR, Perkin-Elmer, USA) by the KBr pellet technique, and scanned from 400-4,000 cm^{-1}.

The zeta potentials of $Mg(OH)_2$ and SLSN in the NaCl solution (10^{-3} M) were measured using a ZetaPALS (Brookhaven, New York, USA) with an average value of three separate measurements. Various dissolved organic components in the supernatant were analyzed for total organic carbon (TOC) by a TOC-Vcpn analyzer (Shimadzu Corporation, Japan). The concentration of oil in the wastewater was analyzed with an infrared spectrometer oil content analyzer (Oil460, Beijing, China) and CCl_4 was used to extract oil from wastewater.

4. Adsorption Experiments

An SLSN stock solution was prepared by dissolving 5,000 mg SLSN in 1 L deionized water. Batch adsorption experiments were carried out to test the adsorption of SLSN on the $Mg(OH)_2$ particles. 2.0 g/L of the $MgCl_2$ was mixed with 20 mL of varying SLSN concentration (50-1,000 mg/L) solutions in a set of 150-mL glass Erlenmeyer flasks. The adsorption of SLSN on the in-situ formed $Mg(OH)_2$ particles was tested at different pH values (9.5-12.5) for probing the dependence of SLSN adsorption on solution pH. The pH was adjusted to the desired values with 0.1 M HCl or 0.1 M NaOH using a pH meter (PB-10, Sartorius, Germany). The mixtures were shaken with a thermostatic shaker (SHZ-82, Jintan, China) at 150 rpm and at different temperatures (298, 318, and 333 K) and centrifuged at 6,000 rpm for 10 min with a centrifuge (LG10-2.4A, Jingli, China). The supernatant was analyzed on a UV-visible spectrophotometer (1601, Shimadzu, Japan) at maximum adsorption wavelength of 280 nm for SLSN.

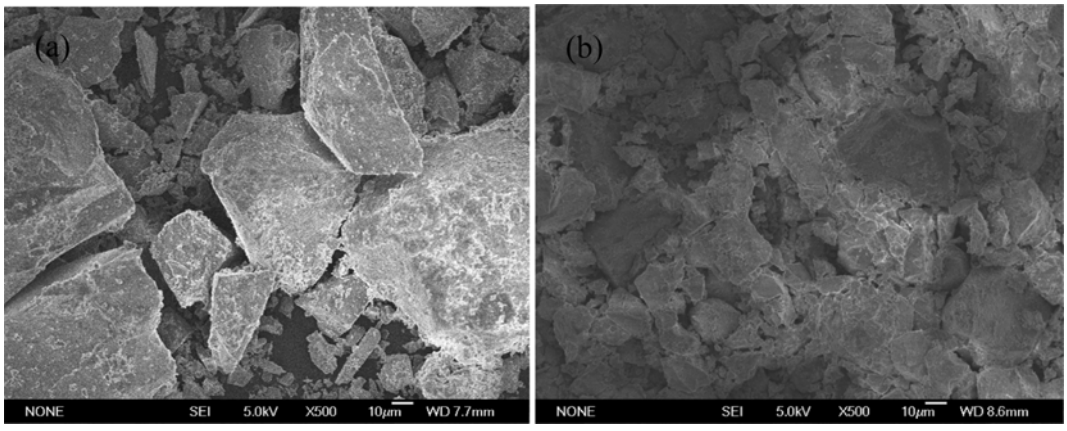

Fig. 1. SEM images of (a) $Mg(OH)_2$, and (b) in-situ formed $Mg(OH)_2$ with SLSN.

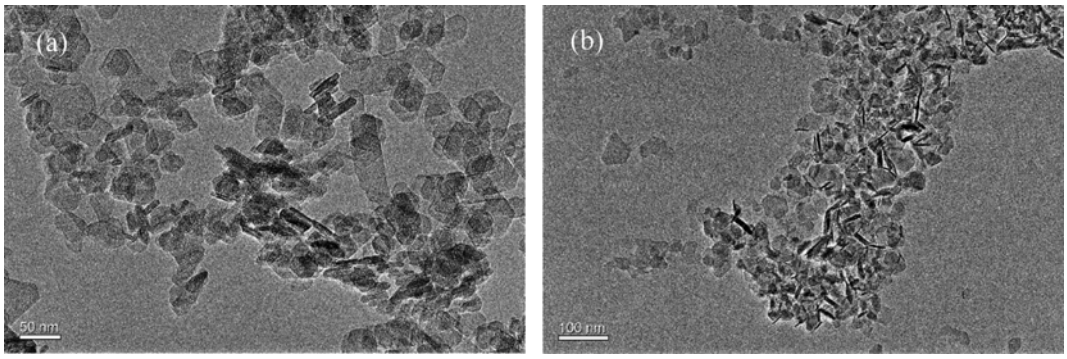

Fig. 2. HRTEM images of (a) $Mg(OH)_2$ and (b) $Mg(OH)_2$-SLSN complexes.

RESULTS AND DISCUSSION

1. Characterization

1-1. SEM

SEM was used to examine the morphology and structure of $Mg(OH)_2$ and after the adsorption of SLSN. SEM images of the in-situ formed $Mg(OH)_2$ with and without SLSN are shown in Fig. 1. From the SEM image (Fig. 1(a)), it can be seen that $Mg(OH)_2$ was composed of smooth, crystalline, and irregularly laminated platelets. Compared to the $Mg(OH)_2$, the $Mg(OH)_2$-SLSN complexes (Fig. 1(b)) showed a more massive and aggregated morphology. This is attributed to surfactant molecules diffusing from the bulk phase to the solid-liquid interface and being adsorbed on the surface of particles. Polar headgroups of surfactant molecules formed chemical bonds with the hydroxyl groups of the $Mg(OH)_2$ particles, and thus the morphology of the $Mg(OH)_2$-SLSN complexes might be changed.

1-2. HRTEM

The morphology and structure of the $Mg(OH)_2$ with and without SLSN were further studied with HRTEM. According to the HRTEM observation (Fig. 2(a)), the $Mg(OH)_2$ crystals appeared to display lamellar-like morphology with diameters of 20-50 nm, and it was confirmed that the freshly formed $Mg(OH)_2$ particles were nanosized. SLSN molecules are dissolved in water and interact with Mg^{2+}, OH^-, and $MgOH^+$ species, leading to adsorption of SLSN molecules on $MgOH^+/Mg(OH)_2$ particles surfaces, and packing into host $Mg(OH)_2$ crystals. $Mg(OH)_2$ tended to form $Mg(OH)_2$-SLSN complexes and then aggregated into large lamellar-like structure through oriented attachment (Fig. 2(b)).

1-3. XRD

The XRD pattern of $Mg(OH)_2$ shown in Fig. 3(a) indicated that the $Mg(OH)_2$ had a layered structure with lattice constants a= 3.147 Å and c=4.772 Å, which are compatible with the reported data (JCPDS card no. 82-2453). Upon adsorption of SLSN on the $Mg(OH)_2$ particles, the basal spacing of in-situ formed $Mg(OH)_2$ with SLSN slightly decreased from 4.85 Å to 4.83 Å (Fig. 3(b)). Furthermore, the density of diffraction peaks became slightly weaker. After adsorption of the surfactant molecules, strong electrostatic attraction and hydrogen bonding between $Mg(OH)_2$ particles and the adsorbed SLSN layer, leading to a slight decrease of the basal spacing.

1-4. FT-IR

FT-IR analysis is an effective method for characterization of $Mg(OH)_2$ and SLSN, and can be used to obtain information about the functional groups and their bonds [30]. The FT-IR spectrum of $Mg(OH)_2$ is given in Fig. 4(a). The strong peak at 3,698 cm^{-1} is assigned to the free hydroxyl group in $Mg(OH)_2$ [31]. A broad and moderate band at 3,459 cm^{-1} is attributed to stretching vibration

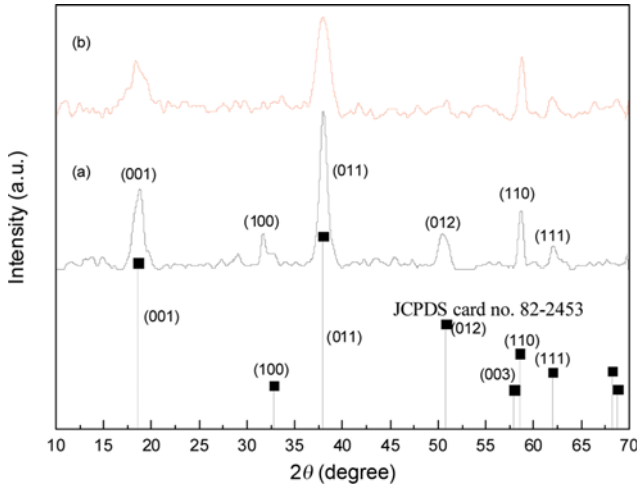

Fig. 3. XRD patterns of (a) $Mg(OH)_2$, and (b) $Mg(OH)_2$ with SLSN.

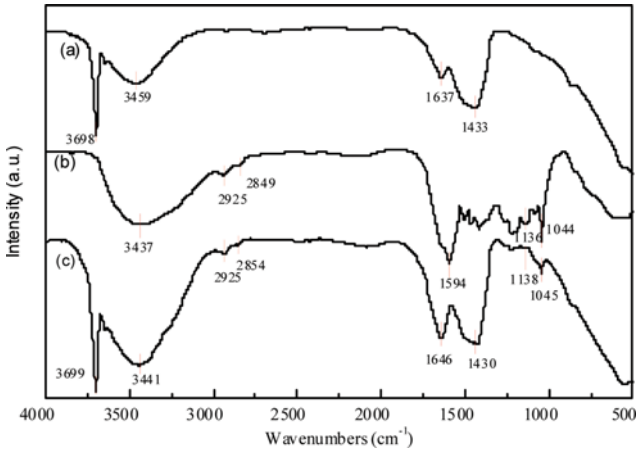

Fig. 4. FT-IR spectra of (a) $Mg(OH)_2$, (b) SLSN, and (c) $Mg(OH)_2$ with SLSN.

of the OH [31,32]. The band at 1,637 cm^{-1} is related to H-O-H bending vibrations of water molecules adsorbed on $Mg(OH)_2$ particles [4]. The adsorption band at 1,433 cm^{-1} shows the presence of carbonate due to a contamination of CO_2 [4].

The FT-IR spectrum of SLSN is given in Fig. 4(b). The band at 3,437 cm^{-1} is assigned to the hydroxyl stretching vibration of SLSN. The bands at 2,925 and 2,849 cm^{-1} are characteristics of -CH_2 asymmetric and symmetric stretching vibrations in the alkyl chains of SLSN [4]. The peak at 1,594 cm^{-1} for SLSN is assigned to the bonding mode of C=O group. The characteristic peaks were observed at 1,136 and 1,044 cm^{-1} corresponding to the stretching vibration and out-of-plane bending vibration of the S=O and -SO_3^{2-} groups of the surfactant molecules, respectively.

The FT-IR spectrum of $Mg(OH)_2$ after adsorption of SLSN is shown in Fig. 4(c). The peak at 3,698 cm^{-1} shifted to 3,699 cm^{-1}, and the band at 3,459 cm^{-1} shifted to 3,441 cm^{-1}, which characterized the effects of the free hydroxyl group and O-H stretching vibration. This indicates the formation of hydrogen bonding between surfactant headgroups and $Mg(OH)_2$ particles. The H-O-H bending vibrations of water molecules shifted from 1,637 cm^{-1} of original $Mg(OH)_2$ to 1,646 cm^{-1} in the $Mg(OH)_2$-SLSN spectrum, while the adsorption band shifted from 1,433 cm^{-1} of original $Mg(OH)_2$ to 1,430 cm^{-1} of $Mg(OH)_2$-SLSN. It is noticeable that a chemical shift of S=O and -SO_3^{2-} groups from 1,136 and 1,044 cm^{-1} of original SLSN to 1,138 and 1,045 cm^{-1} of $Mg(OH)_2$-SLSN occurred, which is possibly attributed to hydrogen bonding [32]. The peak of C=O in SLSN at 1,594 cm^{-1} disappeared in the $Mg(OH)_2$-SLSN spectrum, suggesting that surfactant molecules interacted with $Mg(OH)_2$ particles through electrostatic attraction and hydrogen bonding. Surfactant molecules directly packed into host $Mg(OH)_2$ crystals, and this may result in the disappearance of the peak.

1-5. Zeta Potential Measurements

The changes in zeta potential of $Mg(OH)_2$ particles as a function of pH are shown in Fig. 5, which shows that zeta potential reversal was observed for $Mg(OH)_2$. The isoelectric point (IEP) of $Mg(OH)_2$ particles is about 11.8. For $Mg(OH)_2$, the potential-determining ions are the Mg^{2+} and OH^- ions. The surface charge of $Mg(OH)_2$ particles depends on the composition of their surface layer: $[M^{z+}(OH)_n]^{z-n}$, where z represents the valence of the cation, and n represents the number of the anion [33,34]. At low pH, where z>n, a positive charged surface results because the ratio of Mg^{2+} ions to OH^- ions in the surface layer exceeds 1 : 2. At high pH, where z<n, a negative surface charge results [34]. At pH_{IEP}, where z=n, the $Mg(OH)_2$ particles have a zero net charge.

The pH-dependence on zeta potential of SLSN is presented in Fig. 5. The surface charge increased with an increase in pH values and remained a negative zeta potential within the whole pH range. According to Hunter [35], an increase in ionic strength causes a rise in the Debye-Hückel parameter, k, resulting in a more rapid reduction of the potential with distance. This behavior is referred to as "compression of double layer" and may be responsible for the absolute value of zeta potential to be reduced.

2. Surfactant Adsorption Studies

2-1. Effect of pH

The pH value of the reaction solution is an important parameter that controls surface charge density and dissolution/precipitation of $Mg(OH)_2$. In this study, the pH ranged from 9.5 to 12.5. The concentration of SLSN was 200 mg/L. The effect of pH on the removal efficiency of SLSN on $Mg(OH)_2$ particles is shown in Fig. 6. The removal efficiency of SLSN on the $Mg(OH)_2$ increased with pH until the pH reached 10.5, and then the removal efficiency of SLSN decreased with further increase of pH.

Note that different pH values led to different species distribution for $MgCl_2$ (Visual MINTEQ ver. 3.0) [36]. For the $Mg(OH)_2$-H_2O system, the dominant species at the solid-liquid interface are Mg^{2+}, $MgOH^+$, and $Mg(OH)_2$, as illustrated by the speciation diagram presented in Fig. 7. The concentration of Mg^{2+} remained almost constant at pH<9.48, but abruptly decreased at pH>9.48. When the pH value was between 9.48 and 11.3, Mg^{2+}, $MgOH^+$, and $Mg(OH)_2$ simultaneously existed in the reaction system. This behavior can be attributed to the hydroxylation of Mg^{2+} ions and the protonation of $Mg(OH)_2$ surface sites, leading to formation of

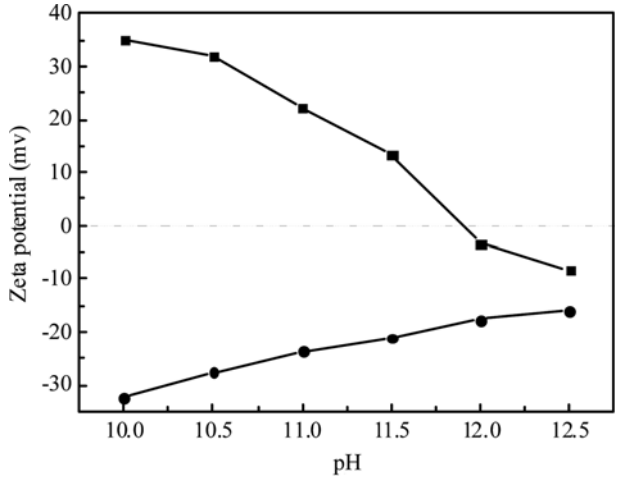

Fig. 5. Zeta potential of (a) $Mg(OH)_2$, and (b) SLSN as a function of pH at 25 °C.

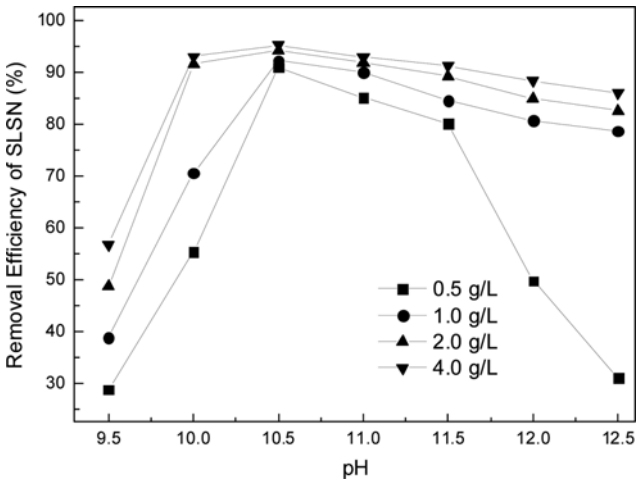

Fig. 6. Effect of pH on the removal efficiency of SLSN on $Mg(OH)_2$ (Experimental conditions: $MgCl_2$ concentration=0.5-4.0 g/L, initial SLSN concentration=200 mg/L, contact time=2 min at 298 K).

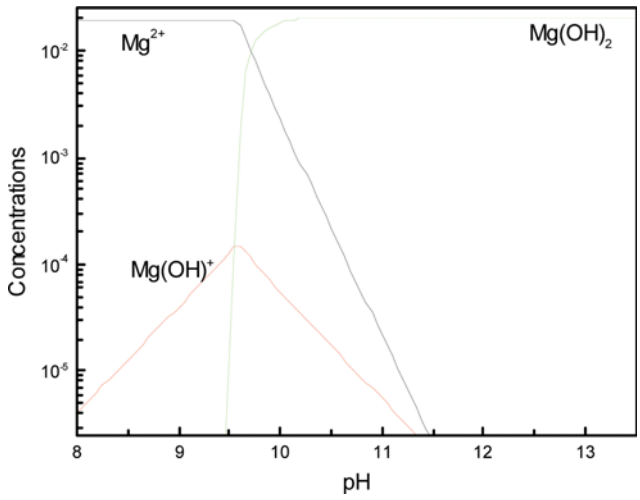

Fig. 7. Species distribution diagram for 2.0 g/L $MgCl_2$ in the pH range from 8.0 to 13.5.

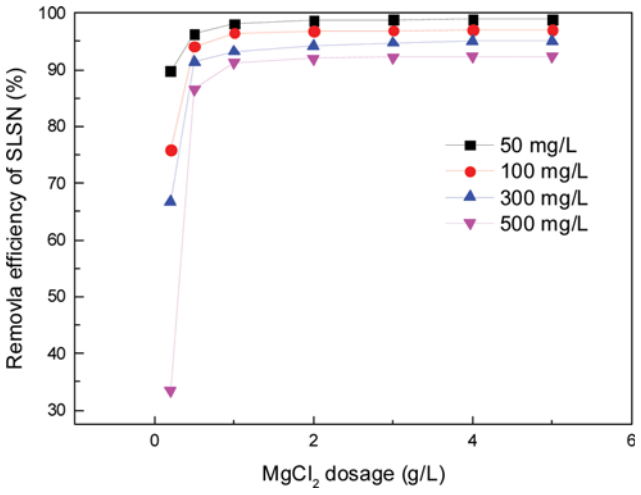

Fig. 8. Effect of $MgCl_2$ concentration and initial SLSN concentration on the removal efficiency (Experimental conditions: initial SLSN concentration=50-500 mg/L, pH=10.5, contact time=2 min at 298 K).

$MgOH^+$ species, which achieved a maximum concentration at pH 9.48. At pH above 11.5, the predominant species was $Mg(OH)_2$.

In-situ formed $Mg(OH)_2$ particles under alkaline conditions may be explained by the following chemical reaction:

$$Mg^{2+} \underset{H^+}{\overset{OH^-}{\rightleftharpoons}} Ma(OH)^+ \underset{H^+}{\overset{OH^-}{\rightleftharpoons}} Mg(OH)_2 \quad (1)$$

At pH 10.5, the predominant species are Mg^{2+}, $MgOH^+$, and $Mg(OH)_2$ species. A considerable increase in positive charge takes place for Mg^{2+} and $MgOH^+$ species. In this case, the zeta potential of $MgOH^+/Mg(OH)_2$ particles can become more positive than that of $Mg(OH)_2$ particles. Therefore, electrostatic attraction between $MgOH^+/Mg(OH)_2$ particles and surfactant molecules increased. At pH values below the IEP, the adsorption mechanism should be primarily electrostatic attraction. In contrast, at pH values above the IEP, electrostatic repulsion between $Mg(OH)_2$ particles and surfactant molecules resulted in a significant decrease in removal efficiency. As maximum removal efficiency of SLSN on $Mg(OH)_2$ was obtained at pH 10.5, we chose pH 10.5 in subsequent adsorption experiments.

2-2. Effect of $MgCl_2$ Concentration

The adsorption of the SLSN on the in-situ formed $Mg(OH)_2$ particles was strongly affected by the initial $MgCl_2$ concentrations. Adsorption experiments were conducted to further investigate the relationship between the adsorption behavior of SLSN and the formation process of $Mg(OH)_2$. The initial SLSN concentrations were 50-500 mg/L. The $MgCl_2$ concentrations ranged from 0.2 to 5.0 g/L at pH 10.5. The adsorption efficiency of SLSN rapidly increased with increasing $MgCl_2$ concentration and then gradually reached a plateau (Fig. 8). This might be associated with crystal growth mechanism of $Mg(OH)_2$. The crystal growth mechanism of $Mg(OH)_2$ might mainly involve three stages: nucleation, growth, and self-assembly [37]. The first stage is nucleation: $MgCl_2$ was ionized and present in the form of Mg^{2+} and Cl^- ions. When alkali was added to solution, OH^- ions and H_2O molecules co-existed in the system, and the H_2O molecules competed with OH^- ions to form Mg-O-H bonds [37]. The association of Mg^{2+} and OH^- ions forms $MgOH^+$ species. When the concentration of $MgOH^+$ species becomes high enough, they aggregate into nuclei. With an increase in $MgCl_2$ concentration, more Mg^{2+} ions are involved in the nucleation process. The second stage is the growth of nanosheets: the OH groups of nuclei might interact with SLSN molecules and agglomerate together by hydrogen bonds and chemical bonds. At the same time, both particle-particle cohesive forces, and SLSN-particle surface adhesive forces are contributed to obtain nanosheets [37]. The adsorption amount of SLSN might rapidly increase during possible growth process. The third stage is self-assembly process: all self-assembly processes could be driven by principle of energy minimization [4,37]. Electrostatic attraction, hydrogen bonding, cohesive and adhesive forces were enough to hold the nanosheets and form $Mg(OH)_2$ crystalline structures [37]. SLSN molecules were adsorbed on the $Mg(OH)_2$ surfaces and packed into host $Mg(OH)_2$ crystals. As other particles close to the SLSN molecules, they also interacted with the SLSN molecules, the alkyl chain of SLSN acted as "bridge" to link neighboring particles. It is possible that SLSN molecules and $Mg(OH)_2$ particles can form a three-dimensional network by orienting adhesive forces, van der Waals forces, electrostatic attraction, and hydrogen bonding [38]. The presence of SLSN molecules in the solution may enhance the nucleation and growth of $Mg(OH)_2$ particles. The co-precipitation/adsorption process occurs during the growth of complex $Mg(OH)_2$ crystals. The $MgCl_2$ concentration plays an important role in the growth rate of nuclei and the amount of $Mg(OH)_2$ formed.

2-3. Effect of Contact Time and Initial SLSN Concentration

The adsorption capacity of SLSN on in-situ formed $Mg(OH)_2$ particles at different initial SLSN concentrations with contact time is shown in Fig. 9. The adsorbed amount of SLSN increased with an increase in contact time and reached complete equilibrium within 2 min. This is a rapid process compared with other adsorptions [39-41].

Because of the presence of water between particles may result in a hydrate shell. Interparticle cohesion may result in capillary forces,

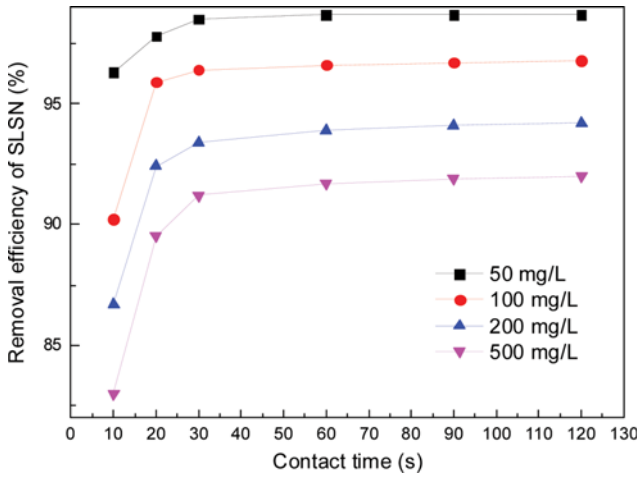

Fig. 9. Effect of contact time and initial SLSN concentration on the removal efficiency (Experimental conditions: initial SLSN concentration=50-500 mg/L, pH=10.5, $MgCl_2$ concentration= 2.0 g/L at 298 K).

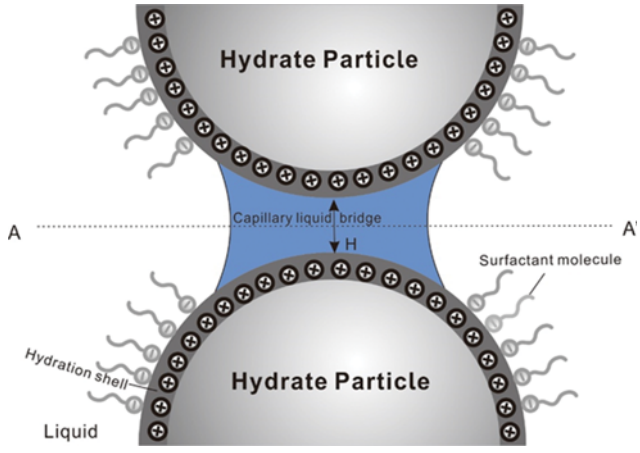

Fig. 10. A schema for the adsorption of SLSN molecules on hydrate particles and interparticle interaction with a capillary liquid bridge cohesion between two hydrate particles, in which AA' is the plane of symmetry. Adapted from Cheng et al. [4] and Aman et al. [42].

which are mainly focused on the condensation of water vapor from the humid atmosphere. When hydrate particles contacted time was longer than 30 s, a "capillary liquid bridge" on the hydrate particle surfaces was created (Fig. 10) [42-44]. Sulfonic acid groups on the surfactant chains may easily interact with the capillary liquid bridge. Moreover, free surfactant molecules diffused from the bulk phase to the solid-liquid interface, and then adsorbed on the $MgOH^+$/$Mg(OH)_2$ particle surfaces. There are adhesive forces between surfactant molecules and hydrate $MgOH^+$/$Mg(OH)_2$ particle surfaces. The adhesive forces are highest when surfactant is hydrophilic [4]. Surfactant molecules can easily adhere to the $MgOH^+$/$Mg(OH)_2$ particle surfaces via adhesive forces. The capillary liquid bridge linked surfactant molecules and hydrate $MgOH^+$/$Mg(OH)_2$ particles to form three-dimensional network via electrostatic attraction, hydrogen bonding, van der Waals forces, and adhesive forces. These forces contributed to the adsorption of SLSN on the $MgOH^+$/$Mg(OH)_2$ particles, and thus time required to reach equilibrium could be much shorter.

The SLSN removal efficiency depends on the concentration of the SLSN (Fig. 9). The percentage of removal efficiency decreased with an increase in initial SLSN concentration. However, the adsorbed actual amount of SLSN on per unit mass of adsorbent increased with increasing SLSN concentration. Moreover, the initial SLSN concentration did not significantly affect the equilibrium time.

3. Adsorption Isotherms

The adsorption equilibrium is important in describing the adsorption behavior. The parameters derived from the representative models provide important data to understand the adsorption mechanism [45]. The experimental equilibrium data of SLSN on the in-situ formed $Mg(OH)_2$ particles were fitted by using Langmuir [46] and Freundlich [47] isotherm models at a fixed temperature and constant pH. These isotherm models give a description of the adsorption equilibrium between the surface active sites of the adsorbent and an adsorbate in solution.

3-1. Langmuir Isotherm

This model supposes that adsorption occurs at homogeneous sites on the adsorbent surfaces, and when a surface site is occupied by an adsorbate, further adsorption cannot occur at this site [46]. The Langmuir isotherm equation can be expressed by the following relationship:

$$q_e = \frac{K_L q_{max} C_e}{1 + K_L C_e} \quad (2)$$

where q_e (mg/g) is the equilibrium adsorption amount of SLSN on the $Mg(OH)_2$ particles, q_{max} (mg/g) is the maximum monolayer adsorption capacity of the adsorbent, K_L is the Langmuir equilibrium parameter, which is related to the adsorption energy and corresponds to the binding affinity between the adsorbent surface sites and adsorbates, and C_e (mg/L) is the equilibrium concentration of SLSN in solution.

3-2. Freundlich Isotherm

The Freundlich isotherm model is an empirical equation implying that the adsorption process occurs on a heterogeneous surface

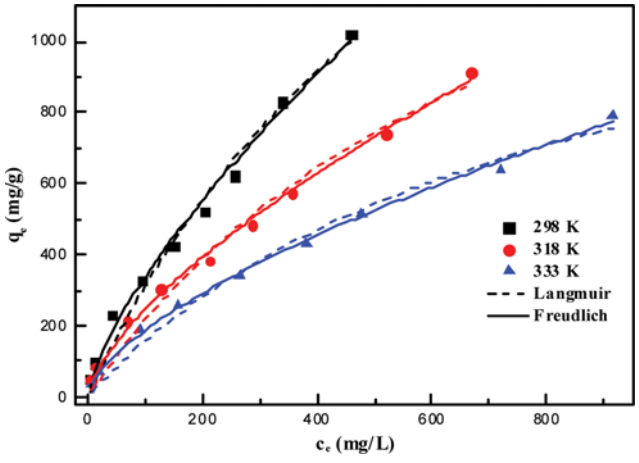

Fig. 11. Adsorption isotherms of the SLSN on the $Mg(OH)_2$ particles at pH 10.5.

Table 1. Langmuir and Freundlich parameters for adsorption of SLSN on the $Mg(OH)_2$ particles

T (K)	Langmuir isotherm			Freundlich isotherm		
	q_{max} (mg/g)	$K_L \times 10^{-3}$ (L/mg)	R^2	K_F	n	R^2
298	2638.76	1.33	0.9769	12.15	1.39	0.9907
318	1936.95	1.25	0.9788	10.75	1.47	0.9946
333	1436.15	1.21	0.9831	9.63	1.55	0.9971

[47]. The Freundlich isotherm can be given by the following equation:

$$q_e = K_F C_e^{1/n} \quad (3)$$

where K_F (L/mg) and n are the Freundlich parameters, which refer to the distribution of active sites and adsorption effectiveness, respectively.

Fig. 11 shows the adsorption isotherms of SLSN on the in-situ formed $Mg(OH)_2$ particles at 298 K, 318 K, and 333 K, which reveals the relationship between the specific equilibrium amount of SLSN on the $Mg(OH)_2$ particle surfaces and the equilibrium concentration of SLSN in solution. The values of the isotherm parameters are listed in Table 1. The parameters resulted from the experimental data suggested that Freundlich isotherm model fitted the experimental data better than that of Langmuir isotherm model. This meant that adsorption process took place on a heterogeneous surface by a multilayer adsorption mechanism [48,49]. Moreover, the values for n were higher than unity at different temperatures, indicating that the adsorption binding strength was weak and controlled by weak interactions such as electrostatic attraction, hydrogen bonding, van der Waals forces and adhesive forces [49].

4. Thermodynamic Parameters

Thermodynamic analysis is important for better understanding the energy of the whole adsorption process, because energy change is the driving force of adsorption process [50-52]. To investigate whether the adsorption would take place spontaneously, changes in standard free energy (ΔG^o), standard enthalpy (ΔH^o), and standard entropy (ΔS^o) were determined by the following equations:

$$\Delta G^o = -RT\ln K_d \quad (4)$$

$$\Delta G^o = \Delta H^o - T\Delta S^o \quad (5)$$

where $K_d = q_e/C_e$, is the equilibrium constant, q_e (mg/g) and C_e (mg/L) are the equilibrium adsorption capacity of SLSN on the $Mg(OH)_2$ particles and equilibrium concentration of SLSN in solution, respectively, R is a gas constant (8.314 J/mol·K), and T is the temperature (K) [47,52].

The relationship between the k_d and temperature is given by the van't Hoff equation [53]:

$$\ln K_d = \frac{\Delta S^o}{R} - \frac{\Delta H^o}{RT} \quad (6)$$

where ΔH^o and ΔS^o can be determined from the slope and intercept of plotting $\ln K_d$ versus 1/T, respectively. The thermodynamic parameters for the adsorption of SLSN on the $Mg(OH)_2$ particles at different temperatures are given in Table 2. The standard free energy of the process at all temperatures is negative, suggesting the spontaneous nature of the adsorption process [47,48]. The negative values of ΔG^o decreased as the temperature increased from 298 K to 333 K, indicating that the lower temperature contributes to adsorption. The negative value of ΔH^o (−17.31 KJ/mol) at the investigated temperatures indicates that the adsorption process involves physical interactions, such as electrostatic attraction, hydrogen bonding, van der Waals forces, and adhesive forces. It is possible that binding between the SLSN molecules and the $Mg(OH)_2$ particle surfaces was weak, and the adsorption process was energetically favorable [54-56]. The negative value of entropy change reflects a decrease in the degree of freedom for the adsorbed SLSN molecules at the solid-liquid interface during the adsorption process [56].

Table 2. Thermodynamics parameters for adsorption of SLSN on the $Mg(OH)_2$ particles

T (K)	ΔG^o (KJ/mol)	ΔH^o (KJ/mol)	ΔS^o (J/mol·K)
298	−3.11		
318	−2.24	−17.31	−47.56
333	−1.43		

The interactions between the in-situ formed $Mg(OH)_2$ particles and the SLSN molecules are controlled by a complex mechanism. It is likely that adsorption occurs by (a) electrostatic attraction between the $MOH^+/Mg(OH)_2$ particles and the oppositely charged SLSN molecules; (b) hydrogen bonding between adsorbed surfactant molecules and hydroxyl groups on the $Mg(OH)_2$ particle surfaces; (c) adhesive forces between SLSN molecules and $Mg(OH)_2$ particle surfaces, and (d) van der Waals forces.

5. Effect of Coexisting Anions

Wastewater generally contains common anions such as NO_3^-, HCO_3^-, $H_2PO_4^-$, and SO_4^{2-} [40]. These anions can also adsorb on the $MgOH^+/Mg(OH)_2$ particle surfaces mainly through electrostatic attraction, hydrogen bonding, van der Waals forces, and adhesive forces [57]. They may interfere with SLSN adsorption by $Mg(OH)_2$. Assuming that there will be no removal of these anions during primary treatment, the intervention of coexisting anions on SLSN adsorption was evaluated by considering the original concentrations, e.g., 10-50 mmol/L of NO_3^-, HCO_3^-, $H_2PO_4^-$, and SO_4^{2-} ions used as model competing anions. The results are shown in Fig. 12. Results show that there was no significant change in SLSN adsorption on $Mg(OH)_2$ after adding competing anions of NO_3^-, HCO_3^-, and $H_2PO_4^-$, while SO_4^{2-} produced a slight change in SLSN adsorption on $Mg(OH)_2$ after adding competing anions. This is attributed to the faster diffusion rate of SO_4^{2-} ions than surfactant molecules. This result may indicate that SO_4^{2-} quickly adsorbed on the $Mg(OH)_2$ surface and occupied adsorption sites,

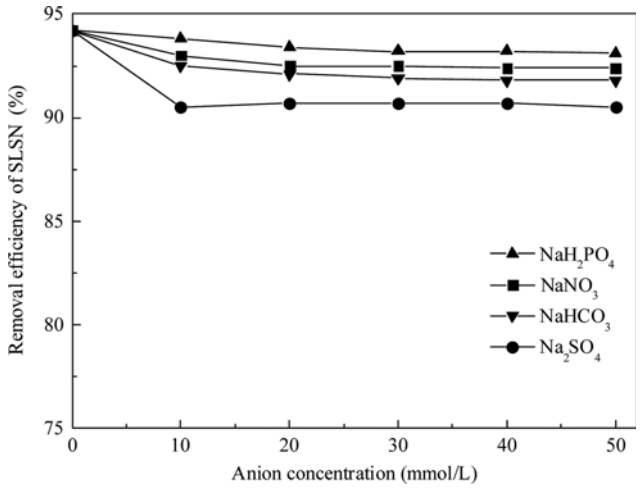

Fig. 12. Effect of coexisting anions on removal efficiency of SLSN on $Mg(OH)_2$ (Experimental conditions: initial SLSN concentration=200 mg/L, $MgCl_2$ concentration=2.0 g/L, pH=10.5 at 298 K).

thus preventing adsorption of SLSN molecules at the solid-liquid interface. There is a strong potential for electrostatic attraction between the SO_4^{2-} ions and the $Mg(OH)_2$ particles in an alkaline solution [57,58]. As a result, a slight decrease in the adsorption capacity of SLSN on $Mg(OH)_2$ was observed. The experiment demonstrated that in-situ formed $Mg(OH)_2$ is not generally affected by the presence of other anions [59]. The in-situ formed $Mg(OH)_2$ has high adsorption selectivity towards SLSN, therefore suggesting its potential application as an adsorbent for SLSN removal from wastewater.

6. Real Wastewater Treatment

Real wastewater was collected from Shengli oilfield ASP flooding produced water. The produced water contained emulsified crude oil, water-soluble polymer (HPAM), surfactant (SLSN), suspended solids, etc. The compositions of the industrial wastewater are illustrated in Table 3, where the average values of each parameter are presented. TOC was determined by a TOC analyzer. The oil concentration in water was measured with an infrared spectrometer oil content analyzer. The suspended solids were determined according to standard procedures [60]. The percentages of the removal efficiency for TOC, oil concentration, and suspended solids are also shown in Table 3. When the $MgCl_2$ concentration increased up to 4.0 g/L at pH 10.5, the in-situ formed $Mg(OH)_2$ had a satisfying TOC and oil removal ability due to hydrogen bonds and chemical bonds formation between polar molecules and the OH groups on the $Mg(OH)_2$ surfaces. TOC and oil removal efficiencies reached 93.5% and 99.3%, respectively, and residual oil was less than 1%. The $MgCl_2$ concentration used in treatment of real wastewater was slightly higher than that in laboratory experiments. It was possible that the presence of oil droplets and water-soluble polymer increased aqueous phase viscosity and facilitated O/W emulsion stabilization.

Table 3. The main characteristic parameters of real wastewater and the percentage of removal efficiency for each parameter

Parameter	Before treatment	After treatment	Percentage of removal (%)
pH	7.8	8.6	——
TOC (mg/L)	418	27.17	93.5
Oil concentration (mg/L)	553	3.87	99.3
Suspended solids (mg/L)	157	0.60	99.6

CONCLUSIONS

$Mg(OH)_2$ particles were prepared by a simple direct aqueous phase precipitation method at a controlled temperature. The IEP of the $Mg(OH)_2$ particles was around 11.8. The experimental data suggested that approximately 93-99% SLSN was removed by in-situ formed $Mg(OH)_2$. The maximum adsorption efficiencies of in-situ formed $Mg(OH)_2$ particles for SLSN were reached within 2 min. The adsorption efficiency increased with increasing pH until pH 10.5, and then the adsorption efficiency of SLSN decreased. The experimental equilibrium data can be well fitted by the Freundlich isotherm. The adsorption process is exothermic, and thus a lower temperature is favorable. When NO_3^-, HCO_3^-, $H_2PO_4^-$, and SO_4^{2-} ions were simultaneously present with SLSN, little competitive adsorption occurred between the other coexisting anions and SLSN molecules for adsorption active sites on $Mg(OH)_2$. The in-situ formed $Mg(OH)_2$ suggested its potential application as an effective adsorbent for the removal of SLSN from aqueous solution. The co-precipitation/adsorption process involves a complex mechanism that is a combination of electrostatic attraction, hydrogen bonding, adhesive forces, and van der Waals forces.

ACKNOWLEDGEMENTS

This work was financially supported by the National Natural Science Foundation of China (No. 51178253). Thanks to Dr. Edward C. Mignot, Shandong University, for linguistic advice.

REFERENCES

1. A. Pal, S. Pan and S. Saha, *Chem. Eng. J.*, **217**, 426 (2013).
2. K. Babu, N. Pal, V. K. Saxena and A. Mandal, *Korean J. Chem. Eng.*, **33**, 711 (2015).
3. J. Zhang, Y. Wang and Q. Peng, *Korean J. Chem. Eng.*, **30**, 1284 (2013).
4. L. Cheng, L. Ye, D. Sun, T. Wu and Y. Li, *Chem. Eng. J.*, **264**, 672 (2015).
5. X. Liu, Y. Zhao, Q. Li, T. Jiao and J. Niu, *J. Mol. Liq.*, **216**, 185 (2016).
6. P. Jiang, N. Li, J. Ge, G. Zhang, Y. Wang, L. Chen and L. Zhang, *Colloid Surf. A*, **443**, 141 (2014).
7. H. Gong, X. Xin, G. Xu and Y. Wang, *Colloids Surf., A*, **317**, 522 (2008).
8. T. Tichelkamp, E. Teigen, M. Nourani and G. Øye, *Chem. Eng. Sci.*, **132**, 244 (2015).
9. A. O. Al-Amodi, U. A. Al-Mubaiyedh, A. S. Sultan, M. S. Kamal and I. A. Hussein, *Can. J. Chem. Eng.*, **94**, 454 (2016).
10. F. Li, W. He, D. Sun, T. Wu and Y. Li, *J. Clean. Prod.*, **104**, 468 (2015).
11. L. Miao, F. Li, D. Sun, T. Wu and Y. Li, *J. Petrol. Sci. Eng.*, **133**, 18 (2015).

12. Z. Adeel and R. G. Luthy, *Environ. Sci. Technol.*, **29**, 1032 (1995).
13. M. L. Cano and P. B. Dorn, *Environ. Toxicol. Chem.*, **15**, 684 (1996).
14. Y. Qin, D. Yang, W. Guo and X. Qiu, *J. Ind. Eng. Chem.*, **27**, 192 (2015).
15. S. Park, E. S. Lee and W. R. W. Sulaiman, *J. Ind. Eng. Chem.*, **21**, 1239 (2015).
16. K. Fox, M. Holt, M. Daniel, H. Buckland and I. Guymer, *Sci. Total Environ.*, **251**, 265 (2000).
17. W. Zou, L. Liu, H. Li and X. Han, *Korean J. Chem. Eng.*, **33**(7), 2073 (2016).
18. T. Karidakis, S. Agatzini-Leonardou and P. Neou-Syngouna, *Hydrometallurgy*, **76**, 105 (2005).
19. C. Henrist, J.-P. Mathieu, C. Vogels, A. Rulmont and R. Cloots, *J. Cryst. Growth*, **249**, 321 (2003).
20. S.-P. Liu, *J. Ind. Eng. Chem.*, **20**, 2401 (2014).
21. J. Yeh, H. Yang and S. Huang, *Polym. Degrad. Stab.*, **50**, 229 (1995).
22. A. Takagaki, M. Sugisawa, D. Lu, J. N. Kondo, M. Hara, K. Domen and S. Hayashi, *J. Am. Chem. Soc.*, **125**, 5479 (2003).
23. J. C. Yu, A. Xu, L. Zhang, R. Song and L. Wu, *J. Phys. Chem. B*, **108**, 64 (2004).
24. W. Jiang, X. Hua, Q. Han, X. Yang, L. Lu and X. Wang, *Powder Technol.*, **191**, 227 (2009).
25. K. T. Ranjit and K. J. Klabunde, *Chem. Mater.*, **17**, 65 (2005).
26. Y. Ding, G. Zhang, H. Wu, B. Hai, L. Wang and Y. Qian, *Chem. Mater.*, **13**, 435 (2001).
27. Y. Diao, W. P. Walawender, C. M. Sorensen, K. J. Klabunde and T. Ricker, *Chem. Mater.*, **14**, 362 (2002).
28. W. Fan, S. Sun, L. You, G. Cao, X. Song, W. Zhang and H. Yu, *J. Mater. Chem.*, **13**, 3062 (2003).
29. X. Lv, M. Li, X. Ma, S. Ma, Y. Gao, L. Tang, J. Zhao, Y. Guo, X. Zhao and Z. Wang, *Colloids Surf., A*, **296**, 97 (2007).
30. Y. Deng, J. B. Dixon, G. N. White, R. H. Loeppert and A. S. Juo, *Colloids Surf., A*, **281**, 82 (2006).
31. P. Wang, C. Li, H. Gong, H. Wang and J. Liu, *Ceram. Inter.*, **37**, 3365 (2011).
32. H. Liu and J. Yi, *Appl. Surf. Sci.*, **255**, 5714 (2009).
33. D. An, X. Ding, Z. Wang and Y. Liu, *Colloids Surf., A*, **356**, 28 (2010).
34. H. Schott, *J. Pharm. Sci.*, **70**, 486 (1981).
35. R. Hunter, Academic Press, London (1981).
36. J. Gustafsson, *KTH Department of Land and Water Resources Engineering, Stockholm, Sweden. Based on de Allison JD, Brown DS, Novo-Gradac KJ, MINTEQA2 ver* **4**, 1991 (2011).
37. F. Li, L. Ye, Y. Li and T. Wu, *RSC Adv.*, **6**, 31092 (2016).
38. S. V. Krishnan and I. Iwasaki, *Environ. Sci. Technol.*, **20**, 1224 (1986).
39. U. F. Alkaram, A. A. Mukhlis and A. H. Al-Dujaili, *J. Hazard. Mater.*, **169**, 324 (2009).
40. M. Doğan, Y. Özdemir and M. Alkan, *Dyes Pigme.*, **75**, 701 (2007).
41. S. Wang and H. Li, *J. Hazard. Mater.*, **126**, 71 (2005).
42. Z. M. Aman, E. P. Brown, E. D. Sloan, A. K. Sum and C. A. Koh, *Phys. Chem. Chem. Phys.*, **13**, 19796 (2011).
43. A. Döppenschmidt and H.-J. Butt, *Langmuir*, **16**, 6709 (2000).
44. Z. M. Aman, K. Olcott, K. Pfeiffer, E. D. Sloan, A. K. Sum and C. A. Koh, *Langmuir*, **29**, 2676 (2013).
45. C. Zhang, S. Yang, H. Chen, H. He and C. Sun, *Appl. Surf. Sci.*, **301**, 329 (2014).
46. I. Langmuir, *J. Am. Chem. Soc.*, **38**, 2221 (1916).
47. H. M. F. Freundlich, *Zeitschrift Für Physikalische Chemie (Leipzig)*, **57**, 385 (1906).
48. C. C. de Escobar, A. Fisch and J. H. Z. dos Santos, *Ind. Eng. Chem. Res.*, **54**, 254 (2015).
49. H. Shakeri, M. Arshadi and J. Salvacion, *J. Colloid Interface Sci.*, **466**, 186 (2016).
50. J. Fan, J. Zhang, C. Zhang, L. Ren and Q. Shi, *Desalination*, **267**, 139 (2011).
51. Y. Zhou, M. Zhang, X. Wang, Q. Huang, Y. Min, T. Ma and J. Niu, *Ind. Eng. Chem. Res.*, **53**, 5498 (2014).
52. C. Li, H. Zhong, S. Wang, J. Xue and Z. Zhang, *J. Ind. Eng. Chem.*, **23**, 344 (2015).
53. K. Gobi, M. Mashitah and V. Vadivelu, *Chem. Eng. J.*, **171**, 1246 (2011).
54. Y. Ho and G. McKay, *Process Saf. Environ.*, **76**, 332 (1998).
55. J. Rawat and D. Singh, *J. Inorg. Nucl. Chem.*, **40**, 897 (1978).
56. L. Zhu, X. Ren and S. Yu, *Environ. Sci. Technol.*, **32**, 3374 (1998).
57. A. M. Moustafa, K. N. McPhedran, J. Moreira and M. Gamal El-Din, *Environ. Sci. Technol.*, **48**, 14472 (2014).
58. J. S. Geelhoed, T. Hiemstra and W. H. Van Riemsdijk, *Geochim. Cosmochim.*, **61**, 2389 (1997).
59. J. Xi, M. He and C. Lin, *Microchem. J.*, **97**, 85 (2011).
60. B. Hansen and S. Davies, *Chem. Eng. Res. Des.*, **72**, 176 (1994).